



Proceedings Article

Configuring magnetoresistive sensor array for head-sized magnetic particle imaging

Suko Bagus Trisnanto ^{a,*} · Tamon Kasajima ^b · Tomohiko Shibuya ^b · Yasushi Takemura ^a

^aDepartment of Electrical and Computer Engineering, Yokohama National University, Yokohama, Japan

^bTechnology and Intellectual Property HQ, TDK Corporation, Tokyo, Japan

*Corresponding author, email: suko-trisnanto-zt@ynu.ac.jp

© 2023 Trisnanto *et al.*; licensee Infinite Science Publishing GmbH

This is an Open Access article distributed under the terms of the Creative Commons Attribution License (<http://creativecommons.org/licenses/by/4.0>), which permits unrestricted use, distribution, and reproduction in any medium, provided the original work is properly cited.

Abstract

Magnetoresistive (MR) sensors offer a solution to enable unidirectional detection of sub-pT signal. Magnetic particle imaging (MPI) can benefit from this high sensitivity to challenge its operability under low excitation fields. Here, we built a prototype of brain MPI scanner by using MR sensor array to directly map stray fields of the magnetized magnetic nanoparticles. The array was a 13×13 matrix with 15 mm sensor pitch and installed at 100 mm apart from excitation coil with 200 mm in diameter. We magnetically compensated both the drive field and geomagnetism to position MR sensor at field-free environment. Preliminarily, we were able to detect a 37 mg_{Fe} ferrofluid sample at 50 mm apart from the array under field amplitudes up to 100 $\mu\text{T}/\mu_0$ at 10 kHz. The resulting noise level appears independent to the applied field, which becomes an advantage to further implement higher drive fields within magnetostimulation safety limits.

1. Introduction

Development of clinical magnetic particle imaging (MPI) triggers a dilemma on how to optimize the amplitude of ac fields applied to magnetic nanoparticles. Standard MPI system typically uses few mT/ μ_0 fields to induce nonlinear field-dependent magnetization response, which leads to harmonic components for encoding tracer location under static field gradient [1]. μ_0 is relative permeability of free space. For instance, a 6 mT/ μ_0 drive field with a 0.2 T m⁻¹ gradient enables imaging of human brain phantom with nearly 1 $\mu\text{g}_{\text{Fe}}\text{mL}^{-1}$ iron content [2]. However, recent study on magnetostimulation effect suggests the use of drive fields below 3.5 mT/ μ_0 as safety limits for brain MPI scanner [3]. Therefore, implementation of sub-mT is preferable to avoid peripheral nerve stimulation, in addition to reducing specific absorption rate (SAR) on human head.

Low field MPI can improve spatial resolution theoretically attributed to insignificant relaxation effects, in

which hysteretic magnetization response with large coercivity potentially induces image blurring [4]. However, tracer sensitivity appears proportional to the applied field [5], thus few mT drive fields within safety limits lead to higher signal-to-noise ratio (SNR). To accommodate sub-pT magnetometry, we proposed the use of ultrasensitive MR sensor as an optional scenario to realize low-field MPI systems. MR sensor itself is applicable to draw quasistatic stray-field map of magnetic nanoparticles, as well as to measure cardiac magnetic fields [6, 7]. Owing to high sensitivity and broad bandwidth of MR sensor, we thus designed an array setup to enable brain MPI scanner in the absence of static field gradient.

II. Material and methods

MR sensor array consisted of a 13×13 matrix to position MR sensors on the corresponding coordinates with 15 mm sensor pitch. TDK Nivio xMR sensor with an over-

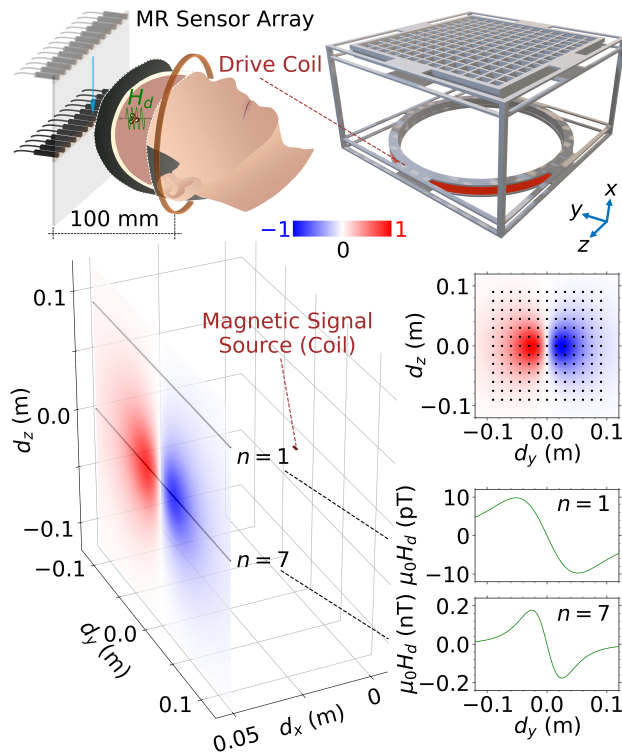


Figure 1: Design of brain MPI scanner using MR sensor array. An excitation coil with 200-mm diameter is placed at 100 mm away from a 13×13 sensor matrix. The array covers $0.18 \times 0.18 \text{ m}^2$ to view field distribution of 1-mm coil installed at 50 mm perpendicularly. The respective H_d field map can be symmetrically obtained from scanning the first row $n = 1$ to $n = 7$ of the array. d_x , d_y and d_z are distances on xyz axes.

all dimension of $12 \text{ mm} \times 12 \text{ mm} \times 74 \text{ mm}$ was supplied by 5 V to acquire $87 \mu\text{V nT}^{-1}$ initial sensitivity. We adopted a monotone magnetometry at 10 kHz, thus either signal amplification or filtering was required to improve the sensitivity up to 20 mV pT^{-1} . To evaluate array coverage, we initially used a 40-turns coil with 1 mm diameter and 5 mm length to generate pT signal. The coil was perpendicularly installed at 50 mm apart from the sensor. We also computed the corresponding spatial field-distribution by using *magpylib* 4.1.1 python package [8].

As shown in Fig. 1, the sensor array was placed 100 mm away from a head-size excitation coil with 200 mm in diameter. The setup requires 169 MR sensors for simultaneous signal acquisition. However, we can reduce to a 1×13 single row and manually scan the stray fields H_d for different rows. The field contour should be symmetrical when the coil was perfectly centered on the array. Thus, moving the 1×13 patch from $n = 1$ to $n = 7$ and joining the patches will fully create field map. Figure 1 (bottom-left panels) roughly estimated lower pT fields across the first row in comparison to the seventh rows. Considering this simulation result, we used TDK Nivio xMR sensor to directly measure stray field of

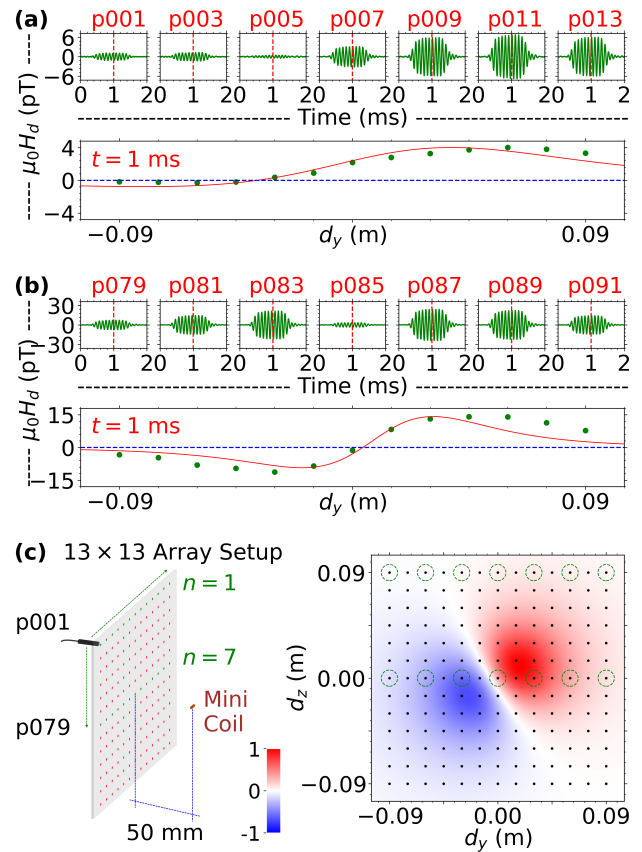


Figure 2: Magnetic field H_d of mini coil measured by MR sensor at (a) first row and (b) seventh row of the array. The coil was fed to a 10-mA current burst at 10 kHz. The sensor readings at $t = 1 \text{ ms}$ for positions p001 to p013 and p079 to p091 estimates (c) spatial field distribution of the coil at 50 mm.

mini coil fed to 10 mA current burst at 10 kHz. The sensor was carefully moved from position p001 to p091, while recording the respective signals for 2 ms with a 12.5 MHz sampling rate.

Similarly, we performed oscillatory magnetometry of a $37 \text{ mg}_{\text{Fe}}$ ferrofluid sample under drive field amplitudes up to $100 \mu\text{T}/\mu_0$ at 10 kHz. In this case, the excessive fields from the excitation coils were magnetically cancelled by installing compensation coils closed to the MR sensor. As preliminary test, we only evaluated sensor at position p085. Regarding spatial resolution, we additionally simulated signal separation of 2 point-sources with different magnitudes.

III. Results and discussion

III.1. Field mapping of mini coil

From Figs. 2 (a) and (b), the field map of mini coil at 50 mm apart appeared asymmetrical due to poor positioning. For $n = 1$, the signals at y axis distance $d_y \geq 0$ (e.g., positions p007 to p013) had higher magnitudes than

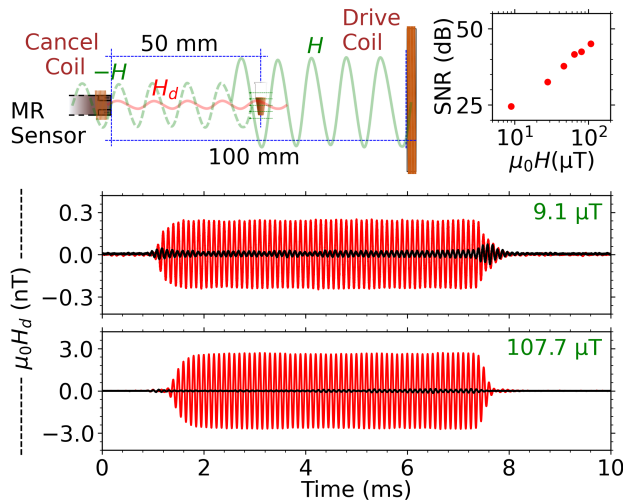


Figure 3: Stray field H_d measurement of 37 mg_{Fe} ferrofluid sample under 9.1 and 107.7 $\mu\text{T}/\mu_0$ drive fields at 10 kHz. The sample was placed in between the array and drive coil. The signal-to-noise ratio SNR (top-right panel) appears proportional to the applied field H .

those at $d_y < 0$ (e.g., positions p001 to p005), although the symmetry appeared to return to normal for $n = 7$. In the case of coil centered on the array, Fig. 1 shows symmetrical field map in which the field is well balanced for both cases of $n = 1$ and $n = 7$. To estimate the spatial distribution, we calculated magnetic field of the coil by rotating it three-dimensionally to fit the sensor readings at arbitrary time $t = 1$ ms. From Figs. 2(a) and (b), the detected pT signals from the coil were identical to the simulated values, thus a full field map can be concluded. Here, Fig. 2(c) confirms the misalignment of the coil relative to the array.

Figure 2 demonstrated that pT signals were detectable by using TDK xMR sensor. The 13×13 array setup further leads to an extended $0.18 \times 0.18 \text{ m}^2$ field of view (FOV) as shown by Fig. 2(c). Since it is unpractical to use 169 sensors simultaneously, signal localization can be cost-efficiently performed by scanning 1×13 or other sub-array configurations. Here, analyzing data from only two 1×13 matrices at $n = 1$ and $n = 7$ were sufficient to locate the signal. We may use a motorized sensor matrix to scan FOV with fewer MR sensors. Nevertheless, large number of sensors leads to better signal localization of phantom with complex geometry and enables real-time imaging. Meanwhile, inductive sensors (i.e., coil array) can also be adopted into MPI system although designing coil array must consider geometrical sensitivity carefully. Large coil diameter increases noise level, whereas small one reduces signal intensity. Here, MR sensor array can minimize crosstalk between sensors since the chip area is very small, as compared to coil array.

III.II. Magnetic nanoparticle detection

Instead of using mini coil, we directly measured the stray fields of the ferrofluid sample under excitation fields below geomagnetism. Since the sensor output was significantly amplified, the dynamic range might be limited to few nT depending on the amplification factor. To avoid output saturation, the current-controlled cancel coils were installed near the sensor to reduce the external field close to zero. We also used self-compensation circuit to tune the residual fields. At 50 mm from the excitation coil, the sample was exposed to the drive field almost twice of that received by the sensor. Thus, for given $100 \mu\text{T}/\mu_0$ to the sample, the sensor will experience $50 \mu\text{T}/\mu_0$, which exceeds dynamic range of the sensor; it was set to ± 10 nT.

From Fig. 3, we were able to recognize magnetization signal of the sample under 9.1 and 107.7 $\mu\text{T}/\mu_0$ drive fields at 10 kHz. The noise level appeared constant below 15 pT, as confirmed at $t > 8$ ms. However, impedance and phase mismatches between cancel field and excessive drive field on the sensor might lead to time-varying signal distortion in the beginning or the end of field burst. We then calculated $\text{SNR} = 20 \log(V_{r,\text{max}}/V_{n,\text{max}})$ to evaluate signal dependency of the applied field. Here, $V_{s,\text{max}}$ and $V_{r,\text{max}}$ are maximum voltage of the detected magnetization signal and ambient noise level, respectively. Shown in Fig. 3 (top-right panel), $V_{s,\text{max}}$ appears linear with the applied field H , which suggests the application of even higher H . In the future, we plan to increase H up to few hundreds $\mu\text{T}/\mu_0$ to confirm whether this output linearity is maintainable. Nevertheless, achievable SNR depends on the specification of compensation coils (i.e., inductance), which may saturate for larger field strength.

The original noise level of TDK Nivio xMR sensor reaches 0.25 pT at 10 kHz. Noisy current fed to the drive coil was responsible for increasing noise level. Even though we were able to reduce 50 μT up to 15 pT at sensor position, magnetization signal of the sample should have low SNR per iron dose. In the case of 37 mg_{Fe} sample under 0.1 mT/ μ_0 (equivalent to 9.5 μAm^2 magnetic moment), the sensor at 50 mm away detected 2.69 nT. In comparison to a mouse-head coil with magnetic moment sensitivity up to 30 fAm² at 320 kHz [9], our system has approximately 53 nAm² at 10 kHz upon 50-mm range particle detection. This moment sensitivity can be improved by increasing the drive field amplitude.

III.III. Spatial Resolution

The use of MR sensor array is aimed to challenge MPI system to reduce either magnetostimulation or SAR effects by using low excitation fields. This scenario may not require spatial encoding since the array readily provides a system matrix (associated with sensor coordinates) for image reconstruction. However, the absence of static field gradient leads to low spatial resolution as signal

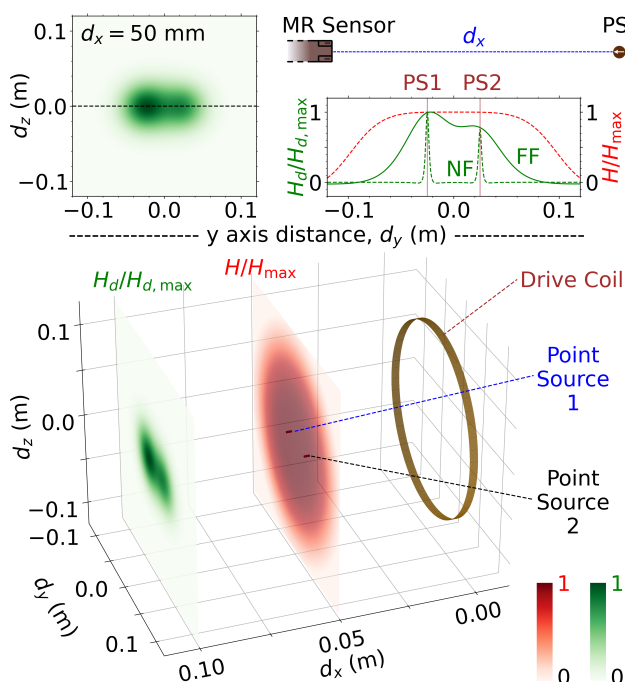


Figure 4: Signal separation of 2 point-sources (PS) simulated at $d_x = 50$ mm away from the array. PS2 has 75 % signal intensity of PS1 and is placed 50 mm nearby. The resulting far-field (FF) map predicts spatial broadening at d_x as compared to near-field (NF) projection at $d_x/10$.

localization becomes physically dependent on the array configuration (e.g., sensor pitch, number of sensors). Furthermore, the broadening far-field (FF) signals with low SNR for a longer distance from their sources is responsible for poor signal separation. From Fig. 4, MPI system with MR sensor array estimates spatial resolution to be equivalent to the distance between sources and the array. Here, 50-mm separated point-sources (i.e., PS1 and PS2) produce overlapping FF signals at $d_x = 50$ mm. The sources are spatially distinguishable from their near-field signals for $d_x = 5$ mm. For further assisting signal localization, we plan to use two orthogonal FF maps on xz and yz planes to estimate correction factor attributed to spatial distribution of the drive fields.

By using MR sensor array, we can expect high temporal resolution equivalent to the applied frequency of the drive field. Since selection fields are unnecessary, temporal resolution is independent to FOV scanning time. We can expect maximum 10000 frames per second (fps) under a continuous 10-kHz drive field for simultaneous signal mapping of all 169 MR sensor outputs. However, record length also limits achievable temporal resolution, in addition to signal acquisition sequences, processing speed, and hardware limitations. In the case of using a 10-ms record length of the tracer signals under a 10-kHz drive-field bursts triggered at 0.2 s interval, temporal resolution is limited to 100 fps.

IV. Conclusion

We built prototype of brain MPI scanner using 13×13 MR sensor array to cover 0.18×0.18 m² FOV. On adopting a multi-patch image reconstruction, we did not perform simultaneous signal acquisition at 169 sensor positions. Instead, we preferably used signals collected from the sensors at a single row as 1D image patch. In the preliminary assessment on mapping stray field of 1-mm coil, the recorded signals were numerically regressed to conclude the spatial distribution of the coil due to asymmetric positioning. Furthermore, direct stray fields measurement of dense ferrofluid revealed the signal linearity to the applied field with relatively constant noise level. This result expects an improved SNR by implementing high drive fields above 0.1 mT/ μ_0 without exceeding magnetostimulation threshold.

Acknowledgments

This work was partially supported by the JSPS KAKENHI Grant Numbers 20H05652 and 22K14268.

Author's statement

Conflict of interest: Authors state no conflict of interest. Informed consent: Informed consent has been obtained from all individuals included in this study.

References

- [1] B. Gleich and J. Weizenecker. Tomographic imaging using the non-linear response of magnetic particles. *Nature*, 435:1214–1217, 2005, doi:<https://dx.doi.org/10.1038/nature03808>.
- [2] M. Graeser, F. Thieben, P. Szwargulski, F. Werner, N. Gdaniec, M. Boberg, F. Griese, M. Möddel, P. Ludewig, D. van de Ven, O. M. Weber, O. Woywode, B. Gleich, and T. Knopp. Human-sized magnetic particle imaging for brain applications. *Nat. Commun.*, 10:1936, 2019, doi:[10.1038/s41467-019-09704-x](https://dx.doi.org/10.1038/s41467-019-09704-x).
- [3] A. A. Ozaslan, M. Utkur, U. Canpolat, M. A. Tuncer, K. K. Oguz, and E. U. Saritas. PNS limits for human head-size MPI systems: Preliminary results. *Int. J. Mag. Part. Imag.*, 8:2203028, 2022, doi:[10.18416/ijmpi.2022.2203028](https://dx.doi.org/10.18416/ijmpi.2022.2203028).
- [4] Z. W. Tay, D. W. Hensley, E. C. Vreeland, B. Zheng, and S. M. Conolly. The relaxation wall: Experimental limits to improving MPI spatial resolution by increasing nanoparticle core size. *Biomed. Phys. Eng. Express*, 3(3):035003, 2017, doi:[10.1088/2057-1976/aa6ab6](https://dx.doi.org/10.1088/2057-1976/aa6ab6).
- [5] Z. W. Tay, D. W. Hensley, P. Chandrasekharan, B. Zheng, and S. M. Conolly. Optimization of drive parameters for resolution, sensitivity and safety in magnetic particle imaging. *IEEE Trans. Med. Imag.*, 39(5):1724–1734, 2020, doi:[10.1109/TMI.2019.2957041](https://dx.doi.org/10.1109/TMI.2019.2957041).
- [6] S. B. Trisnanto, T. Kasajima, T. Akushichi, and Y. Takemura. Long-range stray field mapping of statically magnetized nanoparticles using magneto-resistive sensor. *J. Appl. Phys.*, 131(22):224902, 2022, doi:[10.1063/5.0091365](https://dx.doi.org/10.1063/5.0091365).
- [7] Y. Adachi, D. Oyama, Y. Terazono, T. Hayashi, T. Shibuya, and S. Kawabata. Calibration of room temperature magnetic sensor array for biomagnetic measurement. *IEEE Trans. Magn.*, 55(7):8660661, 2019, doi:[10.1109/TMAG.2019.2895355](https://dx.doi.org/10.1109/TMAG.2019.2895355).

- [8] M. Ortner and L. G. C. Bandeira. Magpylib: A free python package for magnetic field computation. *SoftwareX*, 11:100466, 2020, doi:<https://doi.org/10.1016/j.softx.2020.100466>.
- [9] M. Graeser, P. Ludewig, P. Szwargulski, F. Foerger, T. Liebing, N. D. Forkert, F. Thieben, T. Magnus, and T. Knopp. Design of a head coil for high resolution mouse brain perfusion imaging using magnetic particle imaging. *Phys. Med. Biol.*, 65(23):235007, 2020, doi:[10.1088/1361-6560/abc09e](https://doi.org/10.1088/1361-6560/abc09e).